Supporting Information for

Construction of Nitrogen-Doped Porous Carbon Nanosheets Decorated with Fe-N4 and Iron Oxides by A Biomass Coordination Strategy for Efficient Oxygen Reduction Reaction

Xilong Wang,[a] Chen Yang,[a,b] Peng Guo[c], Yadong Li,[a,b] Nannan Gao,[a,b] Han-Pu Liang[a,b]*

[a]*Key Laboratory of Biofuels, Qingdao Institute of Bioenergy and Bioprocess Technology, Chinese Academy of Sciences, No.189 Songling Road, Laoshan District, Qingdao, 266101, P. R. China*

[b]*Center of Materials Science and Optoelectronics Engineering, University of Chinese Academy of Sciences, No. 19 (A) Yuquan Road, Shijingshan District, Beijing 100049, P. R. China*

[c]*State Key Laboratory of Heavy Oil Processing, China University of Petroleum (East China), Qingdao 266580, P. R. China*

*Corresponding Author.

Tel: +(86) 0532 8066-2638 E-mail: lianghp@qibebt.ac.cn (Han-Pu Liang)

1. Experimental section

1.1 Chemicals

Iron (III) chloride hexahydrate ($FeCl_3$•$6H_2O$), urea, sodium hydroxide (NaOH), and ethanol (99.7%) were purchased from Sinopharm Chemical Reagent Co., Ltd. 20% platinum (HiSPECTM 3000, Pt 20 wt% on carbon black, Johnson Matthey), Nafion solution (5 wt%, DuPont) and polytetrafluoroethylene (PTFE, 60 wt%) were purchased from Hesen Co. Ltd.All of the other chemicals used in this work were analytically pure and were used without further purification. Ultrapure water (resistivity > 18 MΩ cm) was used throughout the experiments.

1.2 Catalysts preparation

The synthesis process of the catalysts is shown in **Figure 1(a)**. Typically, a solution of 0.2 g $FeCl_3·6H_2O$ dissolved in 10 mL of ultrapure water was dropwise added into 30 mg fresh egg white under moderate stirring. After stirring for 3 hours, Fe^{3+} coordinated with the egg white, and yellow colloid was formed. Then, the obtained colloid was sieved through a 0.5 mm mesh and freeze-dried under -50 ^oC on a freeze-drier (Beijing Leading Technology Co., Ltd, FD-1A-50), followed by ground with urea (the mass ratio of colloid to urea is 1:5) using a mortar and pestle for more than half an hour. Finally, the obtained mixture was placed in a quartz boat with 20 cm in length at the center of a 50-mm-diameter quartz tube in a horizontal tube furnace (Tianjin Zhonghuan Lab Furnace Co., Ltd, SK-G018123K) and heated at 800 ^oC, 900 ^oC, or 1000 ^oC for 2 hours with a ramp speed of 5 ^oC min^{-1} under a constant N_2 flow. The as-synthesized samples are denoted as Fe_2O_3@C/FeNC-X, where X represents the heat treatment temperature. For comparison, the electrocatalysts derived from the egg white at 900 ^oC without artificial iron doping was prepared and denoted as NC-900.

1.3 Materials characterization

The morphology and structure of the as-synthesized catalysts were characterized using scanning electron microscopy (SEM) on a Hitachi S-4800 microscope and transmission electron microscopy (TEM) on FEI Tecnai G2 F30 microscope operated at an accelerated voltage of 200 kV. Powder X-ray diffraction (XRD) patterns were collected using a Bruker D8-Advance X-ray diffractometer with Cu Kα radiation (0.1542 nm) at an operating voltage of 40 kV (scan speed 2 and increment 0.02). X-ray photoelectron spectroscopy (XPS) was conducted on a K-Alpha X-ray photoelectron spectrometer (Thermo Fisher Scientific) with Al-Kα micro focused monochromated X-ray source. Raman spectrum was recorded at ambient temperature on a DXR Raman Microscope with 532 nm excitation length. Atomic force microscopy (Multimode 8, AFM) with PFT-QNM mode was carried out to characterize the surface morphology. Nitrogen adsorption/desorption isotherm was obtained on a Micromeritics ASAP 2020 instrument at 77 K. Before each measurement, the sample was evacuated under a vacuum for 3 hours at 150 ^{o}C. The specific surface area was calculated with the Brunauer-Emmett-Teller (BET) method and the pore size distribution (PSD) was calculated from the adsorption branch with the density functional theory (DFT) method. The final Fe content in the best forming catalyst was determined by the inductively coupled plasma optical emission spectrometry (Agilent, ICP-OES730).

X-ray absorption fine structure (XAFS) measurements at Fe K-edge and references were performed at the BL1W1B station in Beijing Synchrotron Radiation Facility (BSRF). XAFS data were collected using a fixed exit double-crystal Si (111) monochromator. The fluorescence signal was collected using a Lytle detector and the energy was calibrated using Fe foil. The acquired EXAFS data were processed using the Athena program in the IFEFFIT software package, and the

data fitting was done by the Artemis program in IFEFFIT.

1.4 Electrode preparation and electrochemical measurements

The electrochemical tests were carried out in a three-electrode system on an electrochemical workstation (CHI760E). A rotating ring-disk electrode (RRDE) with a glassy carbon disk (4 mm diameter) and a Pt ring (5.0 mm inner-diameter and 7.0 mm outer-diameter) served as the substrate for the working electrode for evaluating the ORR performance, while platinum foil was utilized as the counter electrode. The potential was recorded using an Ag/AgCl electrode in saturated KCl as the reference electrode. All of the potentials were calibrated to the reversible hydrogen electrode (RHE) according to the Nernst equation as follow [1]:

$$E\ (vs.\ RHE) = E\ (vs.\ Ag/AgCl) + 0.198 + 0.0592 \times pH \quad (1)$$

To prepare the working electrode, 10 mg catalysts mixed with 40μl Nafion solution (Sigma Aldrich, 5 wt%) were dispersed in 1 ml of ethanol solution by sonicating for at least two hours to form a homogeneous ink. A certain volume of catalyst ink was then drop-casted onto the glassy carbon electrode with a 400 μg cm^{-2} loading for the as-synthesized single-atom Fe catalysts and 100 μg cm^{-2} loading for commercial Pt/C， respectively.

RRDE measurements were conducted by linear sweep voltammetry (LSV) from 1.1 V to 0.2 V vs. RHE at a scan rate of 10 mV s^{-1} at a rotation rate of 1600 rpm in 0.1 M KOH and 0.1 M $HClO_4$ media saturated with O_2, respectively. The background currents of these electrocatalysts in N_2-saturated electrolyte have been deducted. The ring electrode was held at 1.45 V vs. RHE and the H_2O_2 collection coefficient at the ring in RRDE experiments was 0.37. The following equations were used to calculate n (the apparent number of electrons transferred during ORR) and H_2O_2 (%) (the percentage of H_2O_2 released during ORR) [2].

$$n = 4 \times \frac{I_d}{I_d + I_r/N} \quad (2)$$

$$H_2O_2\% = 200 \times \frac{\frac{I_r}{N}}{I_d + \frac{I_r}{N}} \quad (3)$$

where I_d is the faradaic current at the disk, I_r is the faradaic current at the ring and N is the H_2O_2 collection coefficient at the ring.

The kinetic current densities (J_k) involved during the ORR process were determined by analyzing Koutecky-Levich (K-L) equation [3]:

$$\frac{1}{J} = \frac{1}{J_L} + \frac{1}{J_k} = \frac{1}{B\omega^{1/2}} + \frac{1}{J_k} \quad (4)$$

$$B = 0.62nFC_oD_o^{2/3}\upsilon^{-1/6} \quad (5)$$

where J is the measured current density, J_k and J_L are the kinetic and diffusion limiting current densities, ω is the angular velocity of the rotating electrode (ω=2πN, N is the linear rotation speed). N is the electron transfer number, F is the Faraday constant (96485 C mol^{-1}), C_o is the bulk concentration of oxygen (1.2×10^{-6} mol cm^{-3}), Do is the diffusion coefficient of oxygen in 0.1 M KOH and 0.1 M $HClO_4$ (1.9×10^{-5} cm^2 s^{-1}), and υ is the kinematic viscosity of the electrolyte (0.01 cm^2 s^{-1} for both the 0.1 M $HClO_4$ solution and 0.1 M KOH solution).

To investigate the catalysts' durability, the chronoamperometry was conducted at 0.67 V for 40000s in O_2-saturated 0.1 M KOH at a rotation speed of 1600 rpm.

Zinc-Air Battery Tests

A home-made zinc-air battery device has been employed for battery performance and stability measurements. The electrolyte used for the rechargeable zinc-air battery was 6 M KOH and 0.2 M $Zn(Ac)_2$ solution. Typically, 5 mg single-atom Fe catalysts mixed with 20 μL Nafion solution (Sigma Aldrich, 5 wt%) were dispersed in 1 ml of ethanol solution by sonicating for two hours to form a homogeneous ink, a certain volume of catalyst ink was then brushed onto a 1.0 cm^{-2} carbon paper

with a catalyst loading of 1 mg cm^{-2}. A polished zinc plate was used as the anode. As a reference material, 20 wt% Pt/C catalysts were prepared as the same procedure and the Pt/C loading on the carbon was 1.0 mg cm^{-2}. Discharge polarization and power density curves were measured on CHI 760E electrochemical workstation (CHI Instruments, Inc., Shanghai). The galvanostatic charge-discharge cycling curves were measured by a LAND multichannel battery testing system.

2. Supporting Figures and Tables

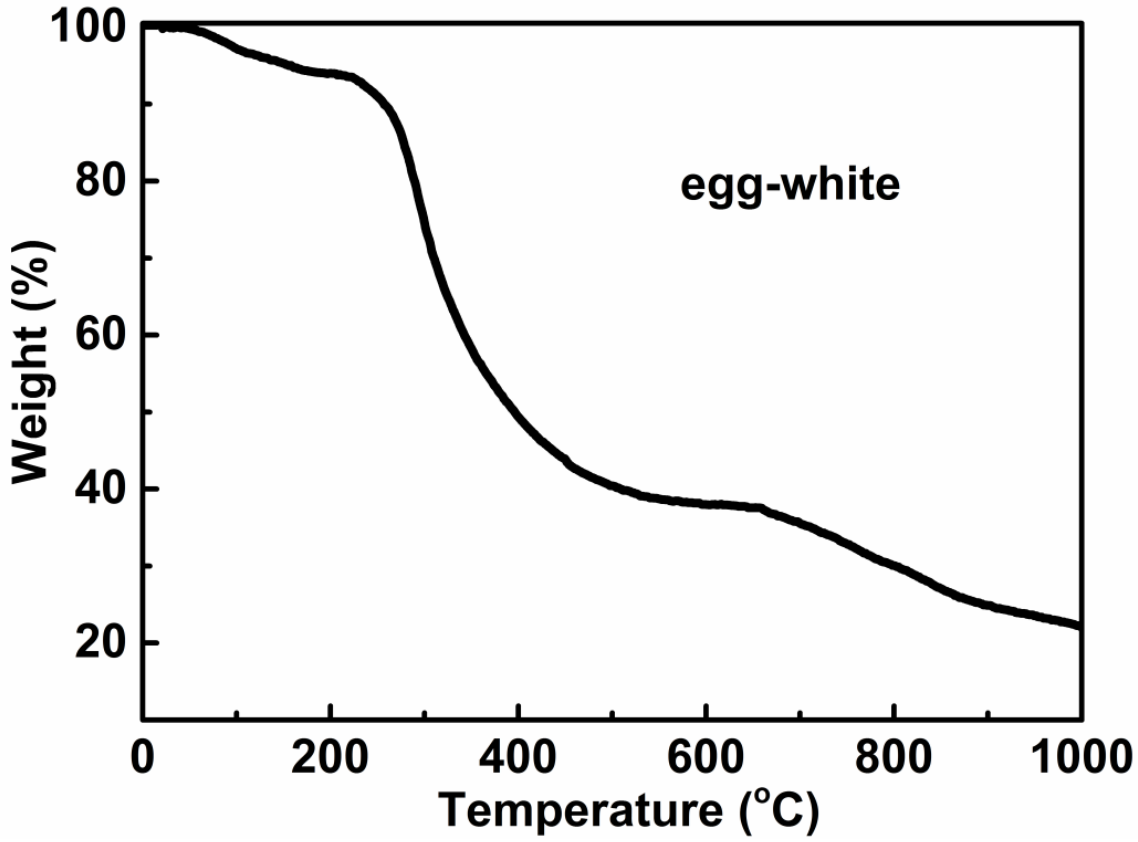

Figure S1. Thermal gravimetric curve of egg-white at a heating rate of 10 ^{o}C min^{-1}.

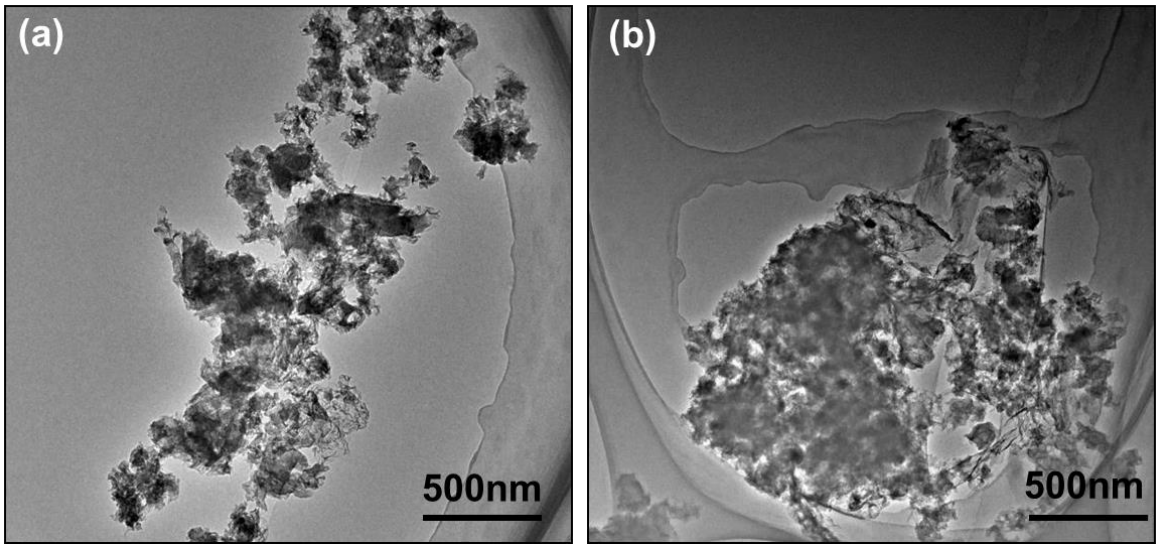

Figure S2. Typical low-magnification TEM images of Fe_2O_3@C/FeNC-900.

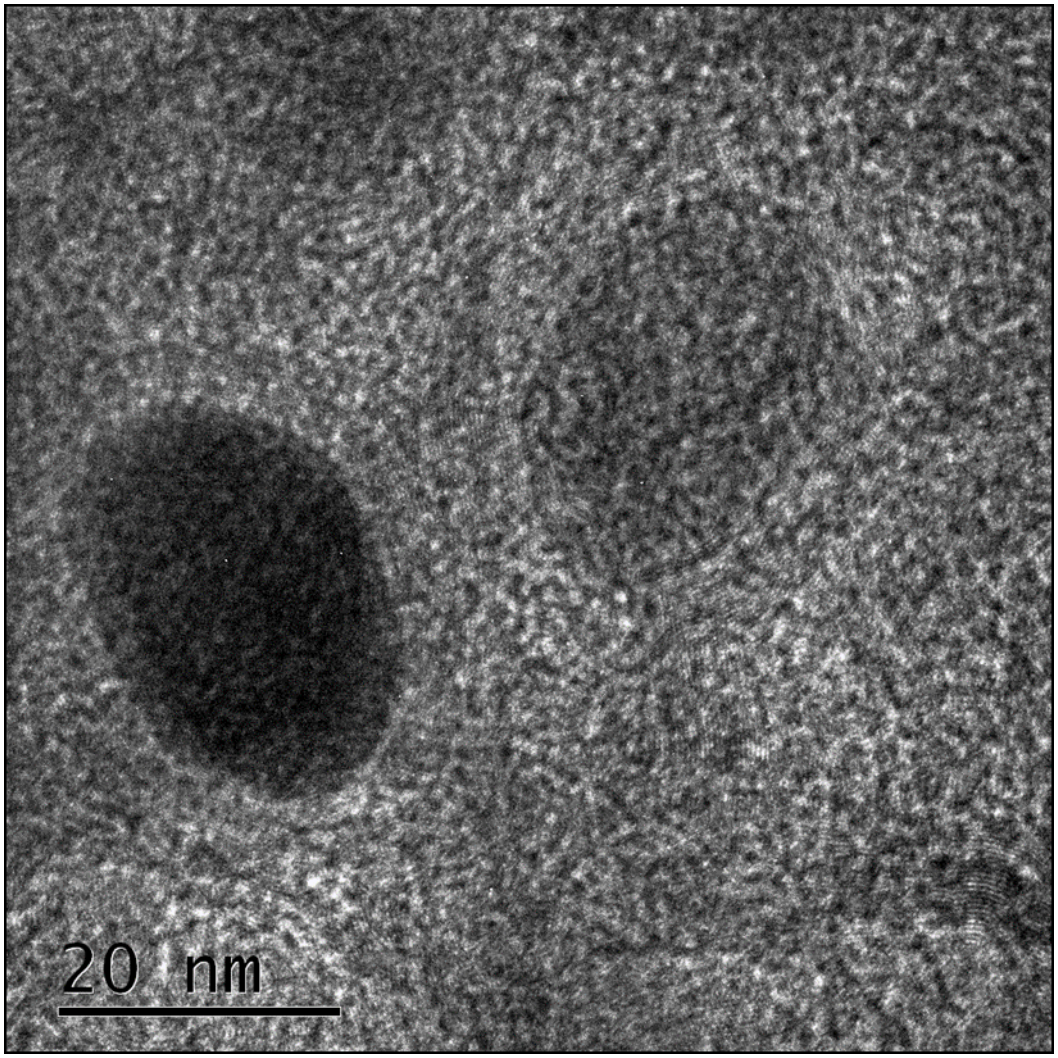

Figure S3. HRTEM images of iron oxides nanoparticles in Fe_2O_3@C/FeNC-900.

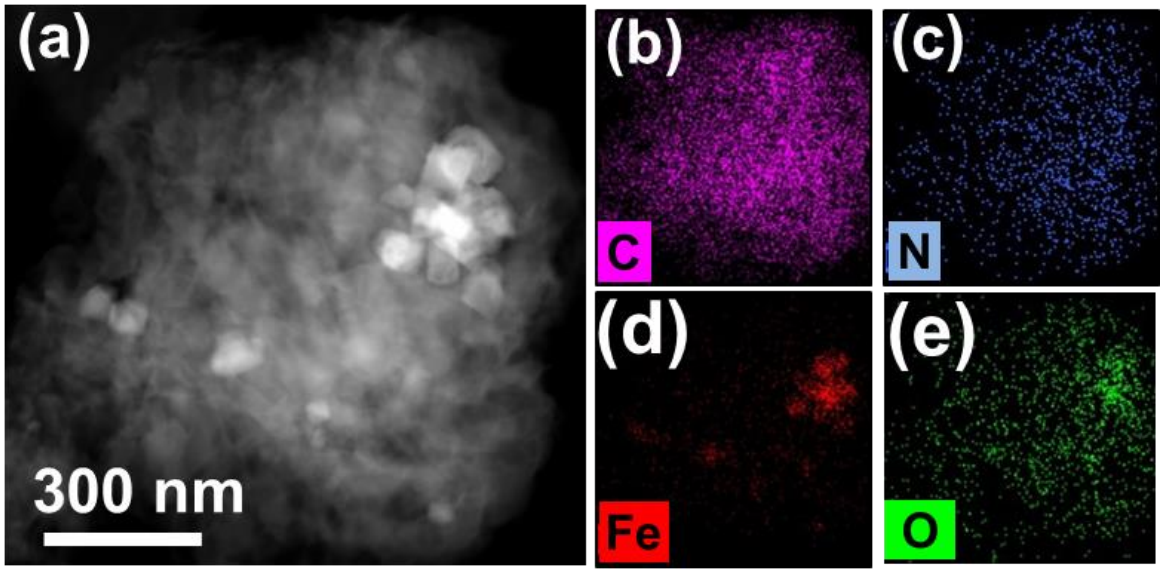

Figure S4. HAADF STEM image of Fe_2O_3@C/FeNC-900 (a) and elemental mapping of (b) C, (c) N, (d) Fe and (e) O.

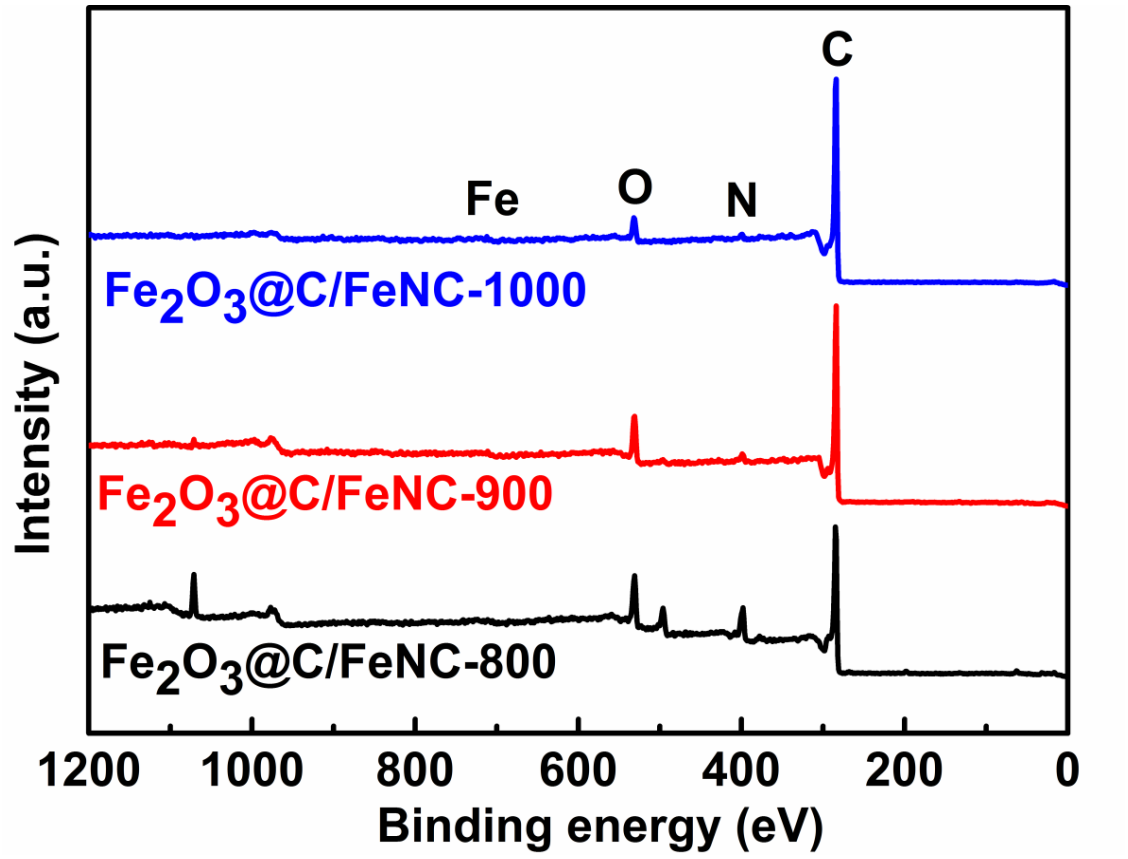

Figure S5. Wide-range XPS spectra of the as-synthesized catalysts pyrolyzed at different temperatures.

Table S1. The contents of C, N, Fe, O (according to XPS analysis) in the as-synthesized electrocatalysts in this work (at %).

Element	Fe_2O_3@C/FeNC-800	Fe_2O_3@C/FeNC-900	Fe_2O_3@C/FeNC-1000
C	71.33	84.05	91.23
N	13.78	3.19	2.77
Fe	0.51	0.49	0.34
O	13.97	11.73	5.48

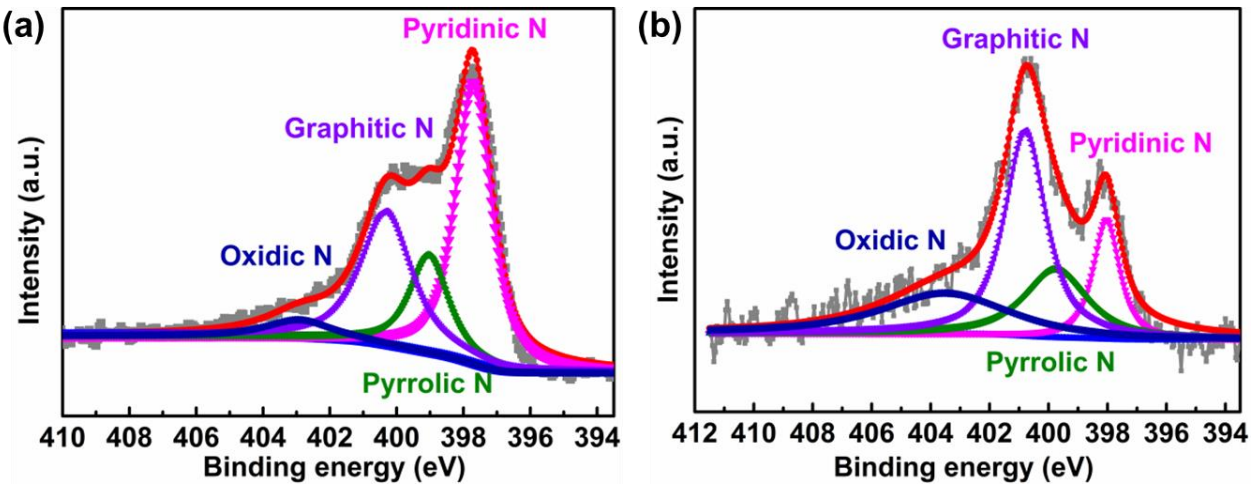

Figure S6. High-resolution N 1s XPS spectra of (a) Fe_2O_3@C/FeNC-800 and (b) Fe_2O_3@C/FeNC-1000.

Table S2. Comparison of nitrogen contents in the as-synthesized catalysts.

Catalysts	Total nitrogen (at. %)	Pyridinic-N (at. %)	Pyrrolic-N (at. %)	Graphitic-N (at.%)	Oxide-N (at.%)
Fe_2O_3@C/FeNC-800	5.14	44.73	17.79	31.76	5.72
Fe_2O_3@C/FeNC-900	3.19	31.19	16.53	43.71	8.57
Fe_2O_3@C/FeNC-1000	2.77	18.04	20.35	45.36	17.99

*Nitrogen content (at.%) evaluated by XPS.

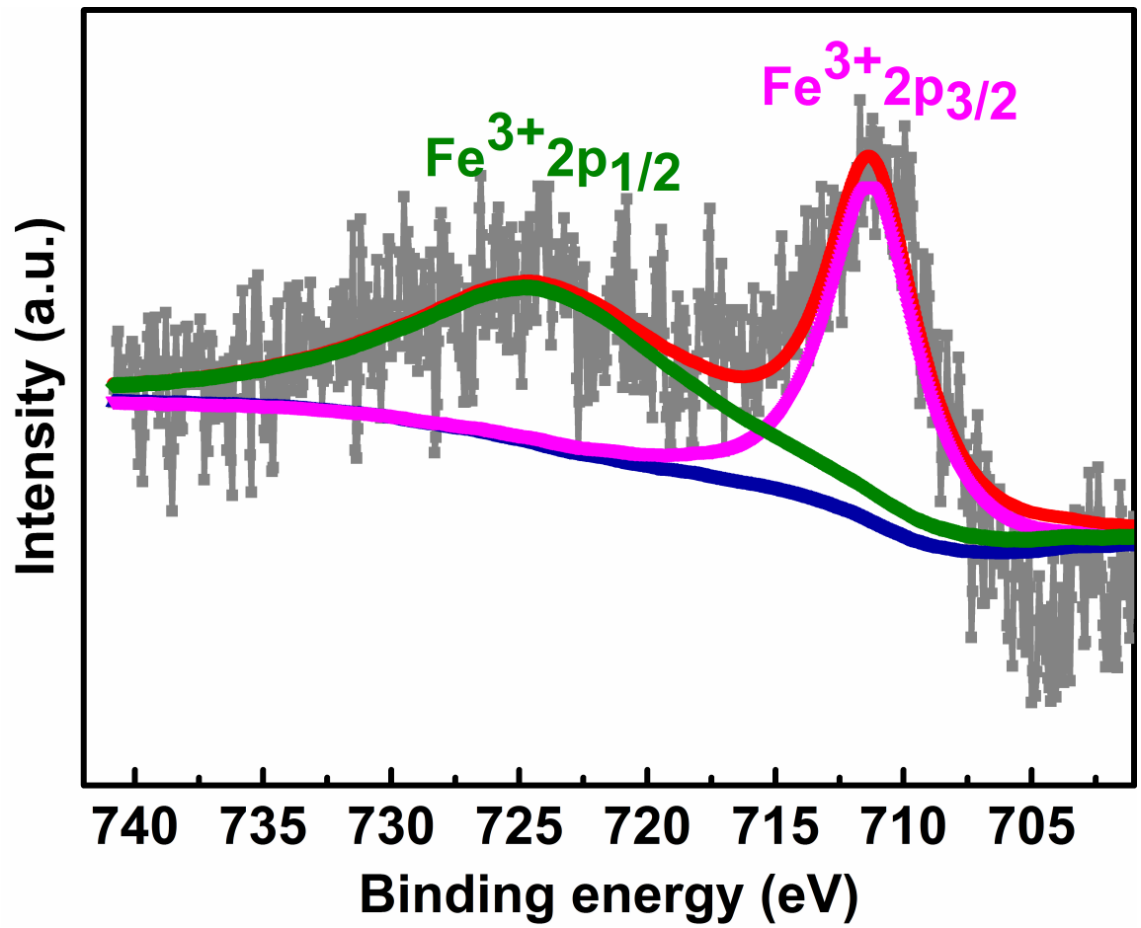

Figure S7. The high-resolution spectrum of Fe 2p of Fe_2O_3@C/FeNC-800.

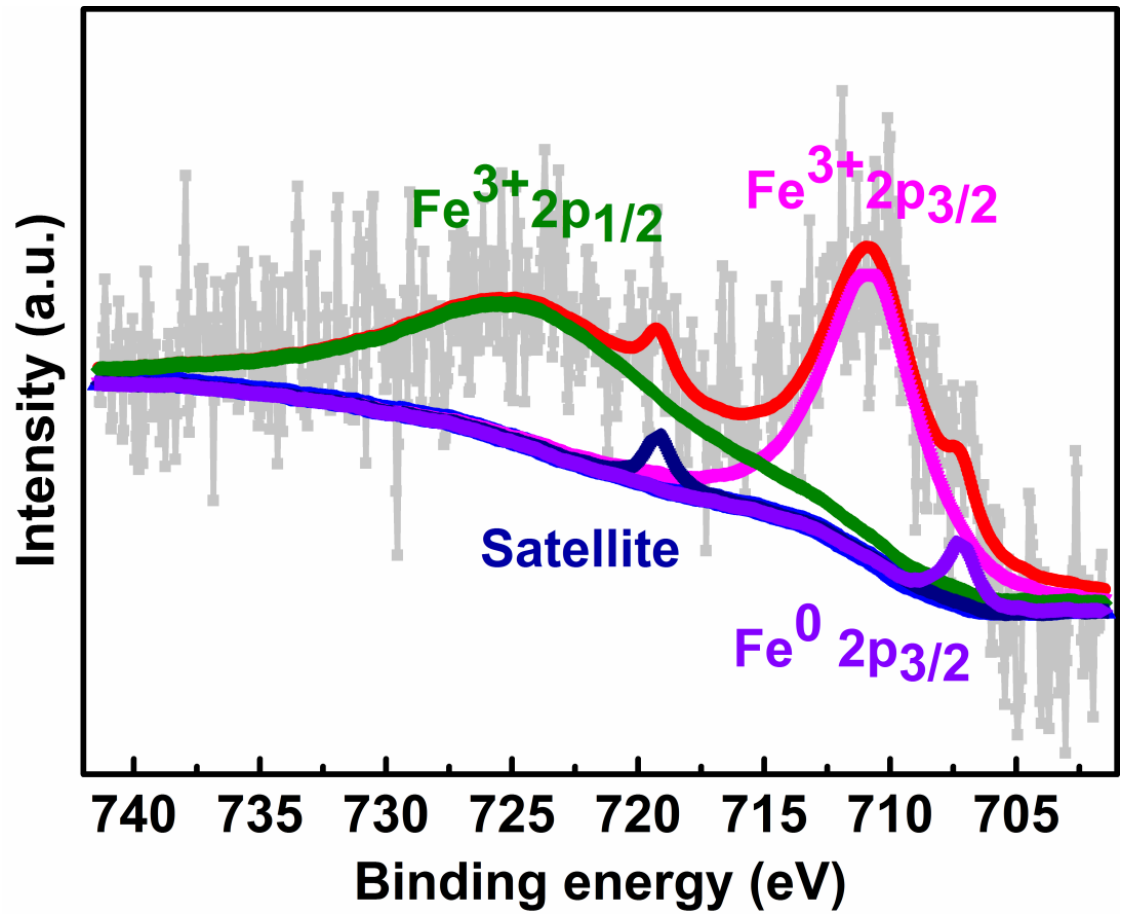

Figure S8. The high-resolution spectrum of Fe 2p of Fe_2O_3@C/FeNC-1000.

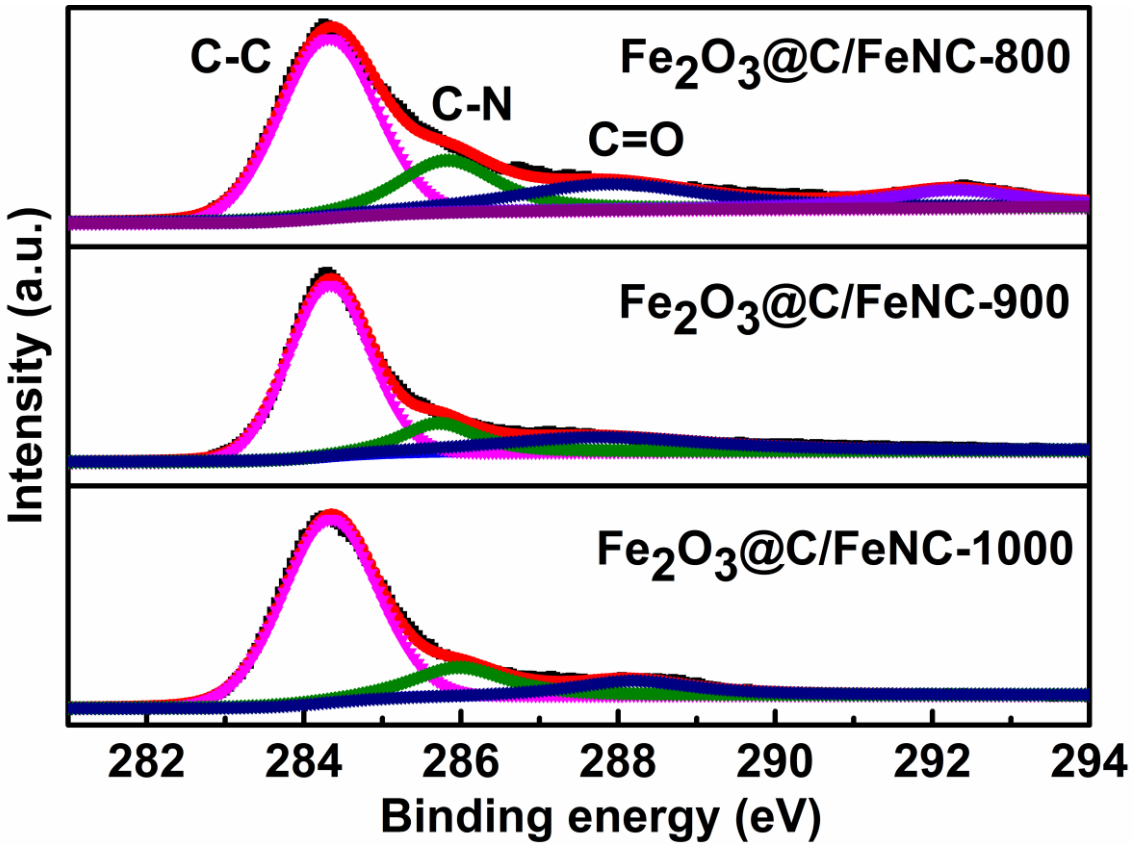

Figure S9. The high-resolution spectra of C 1s of Fe_2O_3@C/FeNC-800, Fe_2O_3@C/FeNC-900 and Fe_2O_3@C/FeNC-1000.

Table S3. Fe K-edge EXAFS curves Fitting Parameters for various samples.

Sample	Scattering pair	CN	R(Å)	σ^2 (10^{-3}Å^2)	ΔE_0(eV)	R factor (%)
Fe foil	Fe-Fe1	8.0±0.8	2.47±0.03	5.6±0.6	3.8±1.0	0.2
	Fe-Fe2	6.0±0.6	2.84±0.02	5.9±0.8		
FeO	Fe-O	6.0±0.8	2.12±0.03	4.4±0.6	2.2±0.6	0.2
	Fe-Fe	12.0±0.8	3.07±0.04	6.4±0.6	3.6±1.0	
Fe_2O_3	Fe-O1	3.0±0.5	1.95±0.02	4.2±0.7	2.1±0.8	0.2
	Fe-O2	3.0±0.5	3.12±0.02	4.4±0.5		
	Fe-Fe1	1.0±0.3	2.90±0.03	5.1±0.7		
	Fe-Fe2	3.0±0.4	2.97±0.03	5.7±0.8	3.5±1.0	
	Fe-Fe3	3.0±0.4	3.64±0.04	6.3±0.8		
Fe_2O_3@C/FeNC-900	Fe-N	4.7±0.1	2.01±0.05	11.1±0.5	-1.2±0.1	0.8

CN is the coordination number; R is interatomic distance (the bond length between central atoms and surrounding coordination atoms); σ^2 is Debye-Waller factor (a measure of thermal and static disorder in absorber-scatter distances); ΔE_0 is edge-energy shift (the difference between the zero kinetic energy value of the sample and that of the theoretical model). R factor is used to value the goodness of the fitting.

S_0^2 is the amplitude reduction factor and was set as 0.85 for Fe-N, which was obtained from the experimental EXAFS fit of FePc reference by fixing CN as the known crystallographic value and was fixed to all the samples.

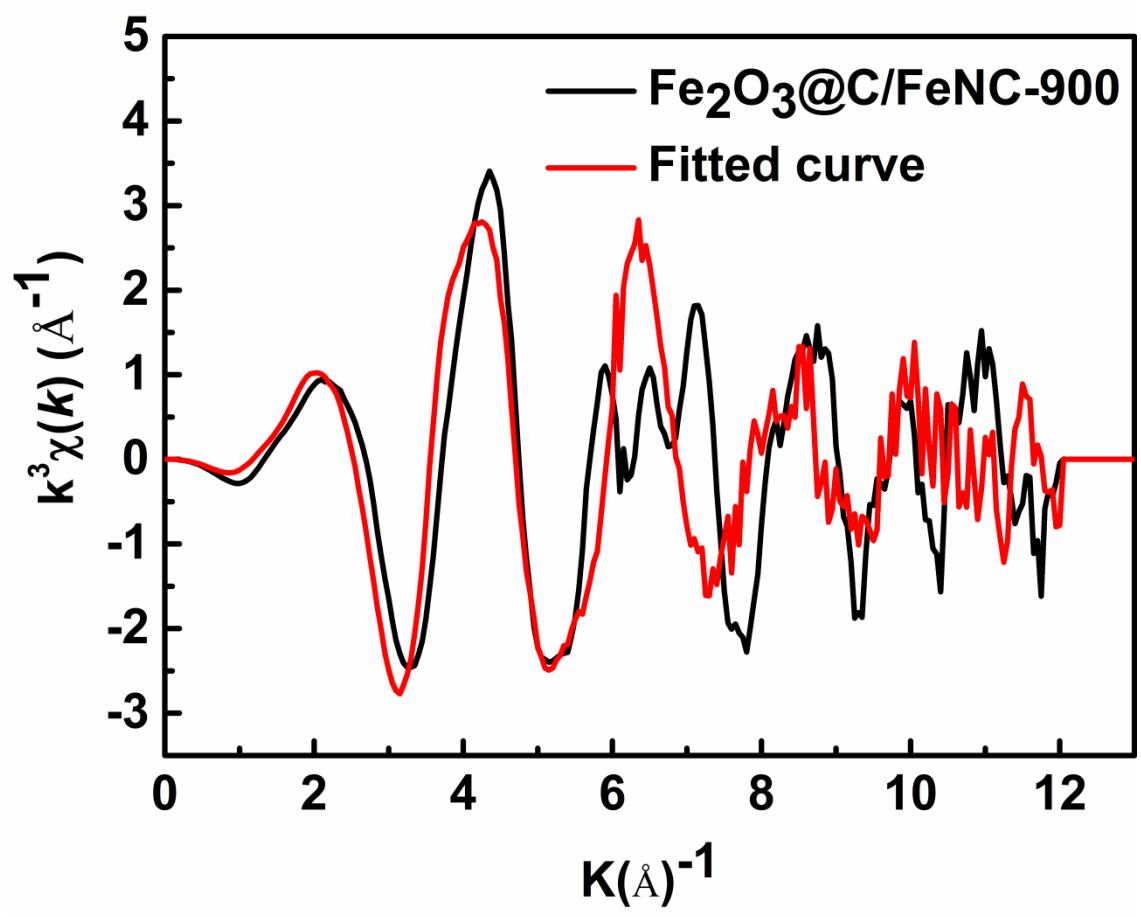

Figure S10. The corresponding EXAFS k-space fitting results of Fe_2O_3@C/FeNC-900

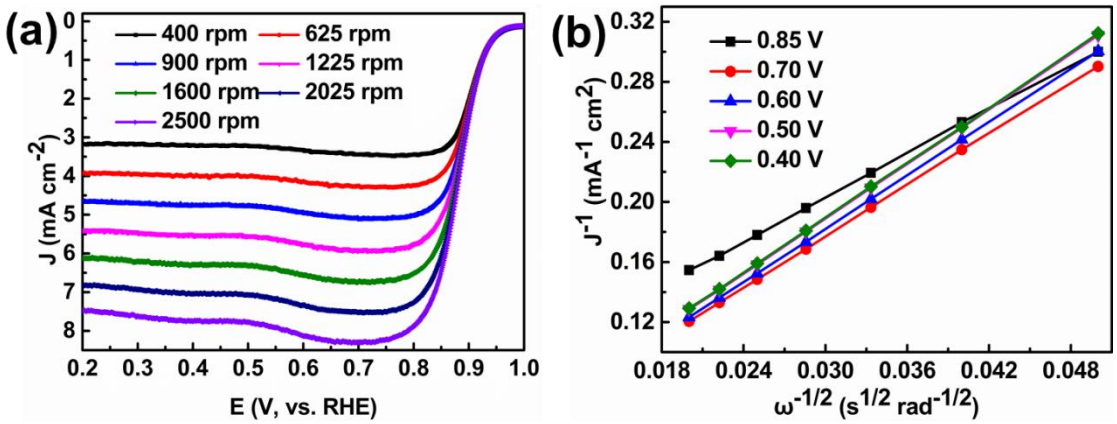

Figure S11. (a) LSV curves of Fe_2O_3@C/FeNC-900 in O_2-saturated 0.1 M KOH at various rotation speeds. (b) K-L plots of Fe_2O_3@C/FeNC-900 at virous potentials.

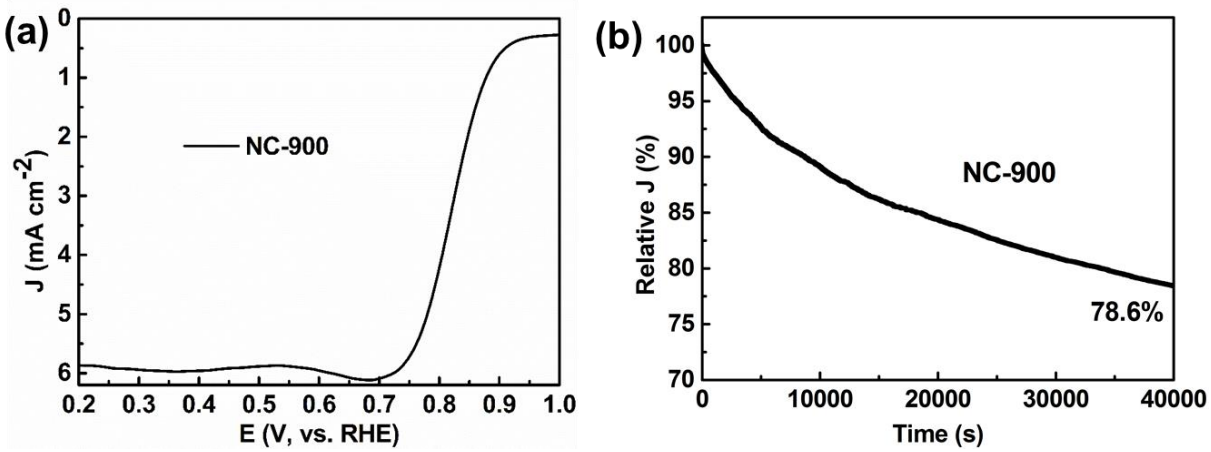

Figure S12. (a) LSV curves of NC-900 in O_2-saturated 0.1 M KOH at rotation speed of 1600 rpm. (b) The i-t chronoamperometric responses of NC-900 and JM Pt/C in O_2-saturated 0.1 M KOH.

Table S4. Comparison of the ORR catalytic activities of some leading nonprecious metal catalysts derived from biomass precursors reported previously and our Fe_2O_3@C/FeNC-900 (as measured in 0.1 M KOH saturated with O_2, electrode rotation speed: 1600 rpm).

Catalyst	E_{onset} (V)	$E_{1/2}$ (V)	J_L (mA cm^{-2})	Tafel slop (mV dec^{-1})	Reference
Fe/N/CNT@PCF	0.87	0.77	4.1	65.8	[4]
SA-Fe/NHPC	-	0.87	5.0	52.0	[5]
NiFe@N-CFs	0.94	0.82	5.8	58.0	[6]
$NPAC_{Co}$	0.87	0.78	5.0	-	[7]
NBSCP	0.95	0.836	5.1	81.7	[8]
Fe-N-CNTs	0.94	0.811	4.9	-	[9]
Co_3O_4/NCMTs-800	0.91	0.78	4.5	42.9	[10]
FeNC-900	-	0.85	5.6	-	[11]
Fe-ISA/NC	1.0	0.89	6.2	59.3	[12]
Fe_2O_3@C/FeNC-900	1.0	0.89	6.1	49.0	This work

Reference

[1] Gabe, R. Ruiz-Rosas, E. Morallon, D. Cazorla-Amoros, Understanding of oxygen reduction reaction by examining carbon-oxygen gasification reaction and carbon active sites on metal and heteroatoms free carbon materials of different porosities and structures. Carbon, 2019, 148, 430-440.

[2] Z. K. Yang, C. M. Zhao, Y. T. Qu, H. Zhou, F. Y. Zhou, J. Wang, Y. Wu, Y. D. Li, Trifunctional Self-Supporting Cobalt-Embedded Carbon Nanotube Films for ORR, OER, and HER Triggered by Solid Diffusion from Bulk Metal. Adv Mater, 2019, 31(12), 1808043.

[3] Z. K. Yang, Y. Wang, M. Z. Zhu, Z. J. Li, W. X. Chen, W. C. Wei, T. W. Yuan, Y. T. Qu, Q. Xu, C. M. Zhao, X. Wang, P. Li, Y. F. Li, Y. Wu, Y. D. Li, Boosting Oxygen Reduction Catalysis with Fe-N-4 Sites Decorated Porous Carbons toward Fuel Cells. Acs Catal, 2019, 9(3), 2158-2163.

[4] M. Li, Y. P. Xiong, X. T. Liu, C. Han, Y. F. Zhang, X. J. Bo, L. P. Guo, *Iron and nitrogen co-doped carbon nanotube@hollow carbon fibers derived from plant biomass as efficient catalysts for the oxygen reduction reaction.* J Mater Chem A, 2015, **3**(18), 9658-9667.

[5] Z. P. Zhang, X. J. Gao, M. L. Dou, J. Ji, F. Wang, *Biomass Derived N-Doped Porous Carbon Supported Single Fe Atoms as Superior Electrocatalysts for Oxygen Reduction.* Small, 2017, **13**(22), 1604290.

[6] Y. L. Niu, X. Teng, S. Q. Gong, Z. F. Chen, *A bimetallic alloy anchored on biomass-derived porous N-doped carbon fibers as a self-supporting bifunctional oxygen electrocatalyst for flexible Zn-air batteries.* J Mater Chem A, 2020, **8**(27), 13725-13734.

[7] M. Zhang, X. Jin, L. Wang, M. Sun, Y. Tang, Y. Chen, Y. Sun, X. Yang, P. Wan, *Improving biomass-derived carbon by activation with nitrogen and cobalt for supercapacitors and oxygen reduction reaction.* Appl Surf Sci, 2017, **411**, 251-260.

[8] D. W. Lee, J. H. Jang, I. Jang, Y. S. Kang, S. Jang, K. Y. Lee, J. H. Jang, H. J. Kim, S. J. Yoo, *Bio-Derived Co2 P Nanoparticles Supported on Nitrogen-Doped Carbon as Promising Oxygen Reduction Reaction Electrocatalyst for Anion Exchange Membrane Fuel Cells.* Small, 2019, **15**(36), e1902090.

[9] N. Cai, S. Xia, X. Zhang, Z. Meng, P. Bartocci, F. Fantozzi, Y. Chen, H. Chen, P. T. Williams, H. Yang, *Preparation of Iron- and Nitrogen-Codoped Carbon Nanotubes from Waste Plastics Pyrolysis for the Oxygen Reduction Reaction.* ChemSusChem, 2020, **13**(5), 938-944.

[10] B. Wang, L. Xu, G. Liu, P. Zhang, W. Zhu, J. Xia, H. Li, *Biomass willow catkin-derived Co3O4/N-doped hollow hierarchical porous carbon microtubes as an effective tri-functional electrocatalyst.* J Mater Chem A, 2017, **5**(38), 20170-20179.

[11] W. J. Jiang, W. L. Hu, Q. H. Zhang, T. T. Zhao, H. Luo, X. Zhang, L. Gu, J. S. Hu, L. J. Wan, *From biological enzyme to single atomic Fe-N-C electrocatalyst for efficient oxygen reduction.* Chem Commun, 2018, **54**(11), 1307-1310.

[12] X. L. Wang, J. Du, Q. H. Zhang, L. Gu, L. J. Cao, H. P. Liang, *In situ synthesis of sustainable highly efficient single iron atoms anchored on nitrogen doped carbon derived from renewable biomass.* Carbon, 2020, **157**, 614-621.